# Low Altitude AUV Terrain Navigation Using an Interferometric Sidescan Sonar

Ove Kent Hagen, Kjetil Bergh Ånonsen and Torstein Olsmo Sæbø
Norwegian Defence Research Establishment (FFI)
P O Box 25, NO-2027 Kjeller, Norway
Email: ove-kent.hagen@ffi.no

***Abstract*—In low altitude operations of the HUGIN 1000-MR autonomous underwater vehicle, the footprint of its multibeam echo sounder (EM 3000) becomes small. Terrain navigation depends on terrain variability to be present within the footprint, and becomes less accurate in these scenarios. The problem is addressed by including interferometric sidescan measurements from the on board synthetic aperture sonar (HISAS 1030). Some preliminary results are presented on the comparison of the position accuracy obtained from terrain navigation using each sensor separately, and for the fusion of the two sensors. The comparison is done on co-registered data collected by HUGIN 1000-MR in variable terrain.**

## I. Introduction

The navigation systems of autonomous underwater vehicles (AUVs) in sustained submerged missions are still challenged today. If not supported by some kind of external positioning system, the position error of a state-of-the-art aided inertial navigation system (INS) for AUVs, such as the navigation system of the HUGIN vehicles [1], grows about 0.1% of travelled distance along a straight line. New techniques are under development for the next generation of the HUGIN navigation system [2], by utilizing any suitable payload sensor for improving navigation.

Terrain navigation is one of these techniques, that enables submerged position updates to the AUV's navigation system. By correlating bathymetric measurements made by the AUV with an a priori digital terrain model (DTM), the terrain navigation algorithms find the best matching position. Several real-time systems already exist, e.g. for the AUV62F [3], the MBARI Dorado mapping AUV [4], and the HUGIN AUVs [5]. Good results from sea-trials with real-time feedback to the AUV's navigation system have been reported in [5] [6] [7]. A sea-trial has recently been made with a HUGIN AUV, where the DTM was constructed in real-time on the AUV, and later used for terrain navigation within the same dive [8].

The background of this paper is the challenges for the terrain navigation techniques in low altitude missions. At low altitude the footprint of the sensors used so far, e.g. the multibeam echo sounder (MBE) and the Doppler velocity log (DVL), become so small that it makes it difficult for the terrain navigation algorithms to converge, or they become less accurate. The HUGIN vehicles can also be equipped with an interferometric synthetic aperture sonar (SAS), which because it is side-looking, has a wide swath even at low altitudes. By combining the use of a down-looking MBE and side-looking interferometric sonars, a large footprint for the terrain navigation algorithms can be maintained even at low altitude.


Fig. 1. HUGIN 1000-MR of the Royal Norwegian Navy, recovered by HU Sverdrup II in the Oslo fjord of Norway

In Section II we give a brief description of the HUGIN 1000-MR, along with its primary bathymetric sensors and its navigation system. A discussion of terrain navigation in low altitude scenarios is given in Section III. A brief introduction is also given to a mathematical model for Bayesian terrain navigation, along with an error covariance model for the bathymetric measurements. In Section IV we present experimental results based on data from the HUGIN 1000-MR of the Royal Norwegian Navy, see Fig. 1, and finally the conclusion is presented in Section V.

## II. HUGIN 1000-MR

The HUGIN 1000-MR is a version of the HUGIN AUVs specially designed for mine hunting. The primary sensor is HISAS 1030 [9], a double-sided interferometric SAS. For optimal performance the SAS requires a very accurate navigation system, which is provided by the HUGIN aided INS. The INS integrates measurements of angular rates and linear accelerations from a navigation grade inertial measurement unit through navigation equations compensating for earth gravity and earth angular rate. If left aided only by a pressure sensor bounding the vertical error, the INS horizontal position error will drift about 1 nm/h. The HUGIN INS is therefore

aided by additional sensor measurements integrated through an error-state Kalman filter. If aided by an accurate and properly calibrated DVL, the position error drift when traveling along a straight line is in the order of 0.1% - 0.2% of distance travelled, depending on the accuracy of the DVL unit used. If the AUV is following a pattern such as the typical search patterns used in mine-counter-measure (MCM) missions, many errors are cancelled out going back and fourth, and the resulting position error drift is substantially lower. For SAS imaging alone, accurate attitude and velocity is crucial, and even in completely autonomous missions without position aiding, this is covered by the DVL-aided INS today. However, to be able to efficiently refind sonar contacts detected in the SAS images for identfication by an optical camera, the position accuracy of the AUV is still challenged. To meet this challenge, the next generation of the HUGIN navigation system will utilize any available and suitable onboard sensor for navigation.

The HUGIN 1000-MR is equipped with several sensors measuring bathymetry, of which all can be used to aid terrain navigation. Here we only consider the use of the EM 3000 multibeam echo sounder and the HISAS 1030 for this purpose. One major challenge when using terrain navigation during MCM missions, is the low altitude. When using the SAS in the detection phase, the altitude of operation is about 20 m, and when using an optical camera in the identification phase, it will only be about 2-8 m depending on the visibility conditions.

The HUGIN 1000-MR also carries a conductivity, temperature and depth (CTD) sensor, which makes it possible to both estimate the sound speed at the AUV's position, and to build estimates of the sound speed profiles (SSP) for the complete mission. This is important for accurate processing of bathymetric measurements.

### A. EM 3000

The EM 3000 uses the Mills cross principle, where a phased array transducer transmits a 300 kHz acoustic signal with a beam wide in the across track direction but narrow in the along track direction. The received signal is then beamformed in the across track direction, using a Fast Fourier Transform (FFT) beamformer to resolve the angles. The time of arrival is resolved using amplitude detection for the inner beams, and phase detection for the outer beams [10]. The EM 3000 then compensates in real-time for roll and pitch of the sensor, and performs ray tracing calculations with an uploaded SSP, computing a local level swath bathymetry for each ping.

Let $\phi_i$ denote the beam angle of the vertical for beam $i$, and $\phi_r$ the AUV's roll angle. The beam angles of EM 3000 are then given by

$$\sin(\phi_i - \phi_r) = \frac{c(i-64)}{df N_v}, \tag{1}$$

where $c$ is sound speed at the sensor, $f$ is the frequency, $d$ is the element spacing, $N_v$ is the length of the FFT, and the integer $i \in [1, 127]$ is the beam index. Bottom detections in the outermost beams are rare, leaving a typical swath-width of about 130 degrees [10], which corresponds to about 4 times the altitude in ground range coverage.

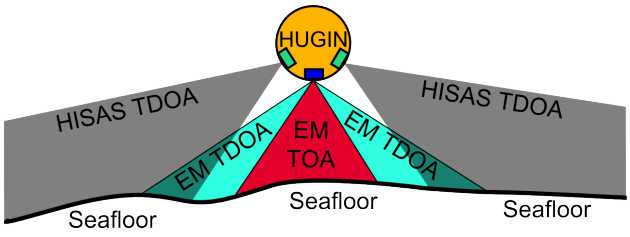


Fig. 2. The HISAS 1030 swath is shown in the gray area, always using time difference of arrival (TDOA) to locate seafloor depth. It overlaps with green areas of the EM 3000 swath, also using TDOA. Time of arrivial (TOA) is used for the centre beams of the EM 3000 shown in the red area.

### B. HISAS 1030

The HISAS 1030 is a sidelooking interferometric SAS sensor [9] which can produce two different bathymetric products: Bathymetry based on SAS images and bathymetry based on sidescan lines. In this paper we only consider sidescan bathymetry.

The HISAS 1030 transmits broad chirp signals around 100 kHz with a ping rate frequency of around 2 Hz. For each transmitted pulse, the echo is received at two vertically separated receivers, which each beamform a single narrow slant-range beam. Then the beams are co-registered by re-sampling them onto a common ground-plane [11]. The differences in two-way travel time between the receivers are estimated by running short cross-correlations along the beams, and then the time-differences are converted to a relative depth measurement. As for the EM 3000, the HISAS 1030 depth measurements are compensated for roll and pitch and for effects induced by the SSP. The depth accuracy is dependent on range and the signal-to-noise ratio, but typically it is better than 5 cm if the SSP is accurately known [11]. However, since the HISAS 1030 observes more horizontally than the EM 3000 it is also more sensitive to SSP-errors [12].

Since the HISAS 1030 is a sidelooking sensor it has a blind-zone directly below the vehicle. On the HUGIN, one HISAS 1030 is mounted on each side. Each HISAS 1030 has a swath from 45 degrees away from nadir and out to 200 meters range. For a typical AUV altitude of 20 meters, this means that the swath is from 20 meters to 200 meters on each side. Since the EM 3000 covers the blind-zone of the HISAS 1030, the two sensors are complimentary and their measurements well suited for fusion, see Fig. 2. The angle of arrival of beam $i$ of HISAS 1030 is given by

$$\sin(\phi_i - \phi_r - \phi_0) = \frac{c\delta\tau_i}{I}, \tag{2}$$

where $\phi_0$ is the installation angle of the HISAS 1030, $I$ is the distance between the receivers, and $\delta\tau_i$ is the time differences for each beam index.

## III. Terrain Navigation

When integrating terrain navigation with an INS, we can distinguish between loosely and tightly coupled integrations.

In the tightly coupled approach the bathymetric measurements are used directly within the filter of the INS, along with all the other sensor measurements. In the loosely coupled approach, the bathymetric measurements are processed in a parallel filter until it converges or diverges, and in case of convergence, the position estimate from terrain navigation is fed back to the INS as a regular position measurement. Here we consider only the loosely coupled approach, but the principles discussed apply to both cases.

Terrain navigation depends completely on the topography, and our knowledge of the topography through a DTM. The estimation problem is as nonlinear as the DTM is, making a characterization of the expected accuracy difficult. The main principle is that the accuracy of the final position estimate depends on the terrain variability within the footprint of the bathymetric sensors. The variability however needs to be on a scale that corresponds with the resolution of the DTM, i.e the variability must also be present in the DTM. In addition, there are cases where even flat parts of the DTM provides important information, as in the case of information about flat sea floor between pockmarks [13]. There are essentially two ways to increase the effective footprint while maintaining the operational altitude; by adding a sensor with a larger ground range coverage, and by collecting enough pings in the direction along the track the AUV is traveling.

### A. Low altitude scenario

The use of both MBEs and 3D sonars have been demonstrated with great success in high precision terrain navigation. The footprint of these sonars in their typical down-looking configuration is limited in low altitude scenarios. For typical mapping missions, where the AUV's altitude is about 40 m, this gives a ground-range coverage up to 160 m with the EM 3000, and is usually sufficient to ensure enough terrain variability within the footprint. The terrain navigation algorithms will usually converge within a few pings and with high accuracy if the terrain variability allows it. However, for the detection-phase of MCM missions at about 20 m altitude, the ground-range coverage of the EM 3000 is decreased to about 80 m. In the identification-phase of the MCM-missions, typically at 5 m and with a ground-range coverage of only 20 m, the accuracy of terrain navigation is substantially lowered, or it takes a substantially longer time to converge.

The inclusion of HISAS 1030 for terrain navigation relieves this problem by providing a 400 m ground-range coverage at 20 m, with a blind-zone that overlaps with the EM 3000 coverage, see Fig 3. At 5 m altitude we will usually not achieve 200 m range from HISAS 1030 because of shadowing and low grazing angles at far range, but nominally 50 m range can be expected (a rule of thumb is that the valid range of HISAS 1030 is 10 times the altitude).

Another way to circumvent the problem is to increase the altitude at some points during the mission, thereby increasing the sensors ground-range coverage. This may be a good strategy for the transit between sonar contacts in the identification phase, but will be an unwanted interference in the detection phase. In covert shallow water missions it may also not be possible to raise the altitude of the AUV without breaching the surface.

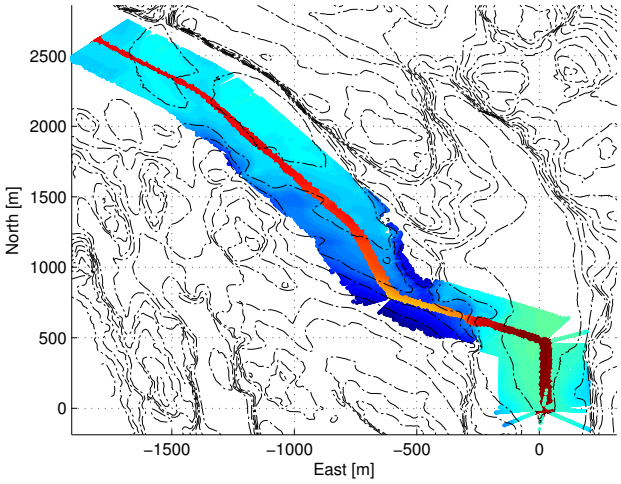


Fig. 3. Bathymetric coverage by the EM 3000 (red/orange), and the HISAS 1030 (blue/green) at about 20 m altitude

### B. Mathematical model

A simplified mathematical model for the dynamics of the AUV and the measurements of the bathymetric sensors is presented to establish a framework for the analysis of the experimental data. Let $\boldsymbol{x}_k = (x_k, y_k, z_k)$ denote the AUV's position in a local north-east-down system at time $t = t_k$. Consider the following dynamical model for the position states of the AUV

$$\boldsymbol{x}_{k+1} = \boldsymbol{x}_k + \boldsymbol{u}_k + \boldsymbol{v}_k, \tag{3}$$

where $\boldsymbol{u}_k$ is the integrated motion estimated by the INS in the time interval $t_k$ to $t_{k+1}$, and $\boldsymbol{v}_k$ is a white stochastic process modeling the error drift in the INS estimate.

Let $(\boldsymbol{\xi}_k, \boldsymbol{\eta}_k, \boldsymbol{\zeta}_k)$ denote $m_k$ bathymetric depth measurements relative to the INS solution in a local level north aligned system, and let $h(x, y)$ denote the global terrain function. We consider the following model for the measurements

$$\boldsymbol{\zeta}_k = \boldsymbol{h}_{\boldsymbol{\xi}_k, \boldsymbol{\eta}_k}(\boldsymbol{x}_k) + \boldsymbol{w}_k. \tag{4}$$

Here we have introduced the measurement vector function $\boldsymbol{h}_{\boldsymbol{\xi}_k, \boldsymbol{\eta}_k}(\boldsymbol{x}_k) = \{h_i\}_{i=1}^{m_k}$ with components defined by

$$h_i = h(x_k + \xi_{k,i}, y_k + \eta_{k,i}) - z_k, \tag{5}$$

and $\boldsymbol{w}_k$ is a stochastic process modeling the bathymetric measurement error. To simplify the model, the additional depth errors caused by errors in the footprint of the measurements, $\boldsymbol{\xi}_k$ and $\boldsymbol{\eta}_k$, have been included in $\boldsymbol{w}_k$.

### C. Point mass filter

The algorithm used in the HUGIN terrain navigation system [5] is based on the point mass filter (PMF). PMF is a nonlinear Bayesian estimator that estimates the probability density function (PDF) of the state on a grid [14] [15]. It was first used in

aircraft terrain navigation [16], but has later made its way into underwater terrain navigation. Before introducing the actual PMF approximation, we consider the Bayesian formulation of the estimation problem (3) and (4).

We define a 2D bounded domain $G_k$ in the earth tangent plane, enclosing the current INS solution. Let $\delta\boldsymbol{x}_k$ denote a position vector in $G_k$ (the error of the INS) with reference to a north-aligned system with origin at the INS solution, and let $Z_k$ denote the set of all measurements between $t_1$ and $t_k$. Our goal is to estimate the position error filter PDF $p(\delta\boldsymbol{x}_k|Z_k)$, conditioned on all the measurements so far in the *correlation period* $[t_0, t_k]$. From (3) we find that $\delta\boldsymbol{x}_k$ is a Markov process, and its PDF evolves in time according to the convolution integral [17]

$$p(\delta\boldsymbol{x}_{k+1}|Z_k) = \int_{G_k} p_{v_k}(\delta\boldsymbol{x}_{k+1} - \delta\boldsymbol{x}_k)p(\delta\boldsymbol{x}_k|Z_k)d\delta\boldsymbol{x}_k, \quad (6)$$

where $p_{v_k}(\cdot) = p(\delta\boldsymbol{x}_{k+1}|\delta\boldsymbol{x}_k)$ is the Markovian transition kernel for the error drift.

The measurement update, following Bayes' theorem, is given by

$$p(\delta\boldsymbol{x}_k|Z_k) = \frac{p_{w_k}(\boldsymbol{\zeta}_k - \boldsymbol{h}_{\boldsymbol{\xi}_k,\boldsymbol{\eta}_k}(\boldsymbol{x}_k + \delta\boldsymbol{x}'_k))p(\delta\boldsymbol{x}_k|Z_k)}{\alpha_k}, \quad (7)$$

where $\alpha_k = \int_{G_k} p_{w_k}(\boldsymbol{\zeta}_k - \boldsymbol{h}_{\boldsymbol{\xi}_k,\boldsymbol{\eta}_k}(\boldsymbol{x}_k + \delta\boldsymbol{x}'_k))p(\delta\boldsymbol{x}_k|Z_k)d\delta\boldsymbol{x}_k$ is a normalization constant, and $p_{w_k}(\cdot)$ denotes the PDF for the sensor measurement error. For notational convenience, we have also introduced the natural 3D extension of the position error, given by

$$\delta\boldsymbol{x}'_k = \begin{pmatrix} \delta\boldsymbol{x}_k \\ 0 \end{pmatrix}.$$

Together the equations (6) and (7) form the recursive Bayesian estimator equations for terrain navigation. The recursion is started by a known initial PDF $p(\delta\boldsymbol{x}_0|Z_0) = p_0(\delta\boldsymbol{x}_0)$ at $t_0$ that depends on the initial INS accuracy, and the filter then runs recursively for each ping until a convergence or divergence criterion is met at $t_K$. The PMF approximation is found by representing the filter PDF by point masses on a regularly spaced grid, and by calculating the integrals through straightforward quadrature. This is the regular way the PMF is run on HUGIN today.

A special solution of (6) and (7) is used in this experiment. We first assume a uniform initial PDF $p_0(\delta\boldsymbol{x}_0) = 1/A_G$, where $A_G = \int_{G_0} d\delta\boldsymbol{x}_0$ is the area of the grid. The error drift in the INS during the correlation period is assumed to be zero, i.e. $p_{v_k}(x) = \delta(x)$, the Dirac delta distribution. In addition the measurement noise is assumed to be Gaussian distributed $p_{w_k} = N(\boldsymbol{0}, \boldsymbol{C}_k)$. In stead of running recursively, all the pings in the correlation period are used in a single batch. By formulating the estimator in this way, both the spatial and temporal correlation between all the measurements in the batch can be modeled without augmenting the state vector. Introducing these assumptions into (6) and (7), the filter PDF can be found as the normalized measurement likelihood

$$p(\delta\boldsymbol{x}_K|Z_K) = \frac{1}{\alpha}\exp\left(-\frac{1}{2}\boldsymbol{d}^T\boldsymbol{C}^{-1}\boldsymbol{d}\right), \quad (8)$$

where $\boldsymbol{d} = \boldsymbol{\zeta'} - \boldsymbol{h}_{\boldsymbol{\xi'},\boldsymbol{\eta'}}(\boldsymbol{x}_K + \delta\boldsymbol{x}'_K)$, and

$$\alpha = \int_{G_K} \exp\left(-\frac{1}{2}\boldsymbol{d}^T\boldsymbol{C}^{-1}\boldsymbol{d}\right) d\delta\boldsymbol{x}_K.$$

The marked measurements are the augmented measurement vectors for the complete batch, given by

$$\boldsymbol{\xi'} = \begin{pmatrix} \boldsymbol{\xi}'_1 \\ \vdots \\ \boldsymbol{\xi}'_k \\ \vdots \\ \boldsymbol{\xi}'_K \end{pmatrix}, \boldsymbol{\eta'} = \begin{pmatrix} \boldsymbol{\eta}'_1 \\ \vdots \\ \boldsymbol{\eta}'_k \\ \vdots \\ \boldsymbol{\eta}'_K \end{pmatrix}, \boldsymbol{\zeta'} = \begin{pmatrix} \boldsymbol{\zeta}'_1 \\ \vdots \\ \boldsymbol{\zeta}'_k \\ \vdots \\ \boldsymbol{\zeta}'_K \end{pmatrix},$$

where each sub vector is compensated for the motion of the AUV during the correlation period. The compensation follows directly from (3), and is given by

$$\begin{aligned} \boldsymbol{\xi}'_k &= \boldsymbol{\xi}_k - \boldsymbol{1}_{m_k}\sum_{j=k}^{K-1} u_{j,x}, \\ \boldsymbol{\eta}'_k &= \boldsymbol{\eta}_k - \boldsymbol{1}_{m_k}\sum_{j=k}^{K-1} u_{j,y}, \\ \boldsymbol{\zeta}'_k &= \boldsymbol{\zeta}_k - \boldsymbol{1}_{m_k}\sum_{j=k}^{K-1} u_{j,z}, \end{aligned}$$

where $\boldsymbol{1}_{m_k}$ is the $m_k \times 1$ vector of ones. A PMF solution to the filter PDF is then found by simply calculating (8) for a set of regularly spaced grid nodes contained in $G_K$. Batch processing was also used in TERCOM [18], and in the maximum likelihood estimator for terrain navigation described in [19]. The batch approximation is here introduced to focus the analysis on the performance of the different sensors in terrain navigation.

### *D. Covariance model*

When mixing different sensors within the same correlation period, it is important to model the covariance of all the measurements, also between the sensors. Consider the following error model for the complete batch of bathymetric depth measurements

$$\boldsymbol{w} = \boldsymbol{w}_z + \boldsymbol{w}_a + \boldsymbol{w}_c + \boldsymbol{w}_h + \boldsymbol{w}_s, \quad (9)$$

where $\boldsymbol{w}_z$ is due to the AUV's depth errors, $\boldsymbol{w}_a$ is due to attitude, alignment and lever-arm errors, $\boldsymbol{w}_c$ is due to sound speed errors, $\boldsymbol{w}_h$ is due to DTM errors, and $\boldsymbol{w}_s$ is due to the sensor processing errors covered in [20] for EM 3000 and in [10] for HISAS 1030. The error component $\boldsymbol{w}_a$ is thoroughly treated in [21], and gives a strong correlation between the measurements. All these error sources are now assumed to

be mutually independent to first order. By computing the covariance matrix of each component, we can then find the final covariance matrix $\boldsymbol{C}$ as the sum of these component matrices. A full derivation of this model is beyond the scope of this paper, but a few of the components are discussed below.

The AUV's depth error is mainly caused by errors in the pressure to depth calculation, typically from errors in compensation of tidal waves, atmospheric pressure, CTD profile and swell. If the depth is derived from pressure in the way recommended in [22], the depth error should be slowly varying, and it is reasonable to assume it is constant within the correlation period. The depth error is then perfectly correlated between all the measurements, with a covariance given by

$$\boldsymbol{C}_z = E[\boldsymbol{w}_z \boldsymbol{w}_z^T] = \sigma_z^2 \mathbf{1}_{m,m}, \tag{10}$$

where $\sigma_z^2$ is the depth error variance, $\mathbf{1}_{m,m} = \mathbf{1}_m \mathbf{1}_m^T$ is the $m \times m$ matrix of ones, and $m = \sum_{k=1}^{K} m_k$ is the total number of measurements in the batch.

The error due to sound speed has two major components. At the sensor the sound speed is used to resolve the angle of arrival, and an estimated SSP is then used to propagate the ray through the water column, compensating for refractions of the sound waves. Any inaccuracies in sound speed will lead to both range and angular errors. We now consider the angular error at the sensor, and assume the sound speed error to be zero-mean and constant within the correlation period, and with a variance denoted by $\sigma_c^2$. Partial derivation of (1) and (2) with respect to $c$ yields

$$\cos(\phi_i - \phi_r)\frac{\delta \phi_i}{\delta c} = \frac{i}{df N_v},\ i \in EM3000 \tag{11}$$

$$\cos(\phi_i - \phi_r - \phi_0)\frac{\delta \phi_j}{\delta c} = \frac{\delta \tau_i}{I},\ i \in HISAS1030 \tag{12}$$

The altitude of the beam $i$ is given by $\zeta_i = r_i \cos(\phi_i)$, where $r_i$ denotes the range to the sea floor along this beam vector. A partial derivation with respect to $c$ gives

$$\frac{\delta \zeta_i}{\delta c} = -r_i \sin(\phi_i)\frac{\delta \phi_i}{\delta c} \tag{13}$$

By introducing (11) and (12) into (13), and rewriting their right hand sides by using (1) and (2), we arrive at a common first order error equation for both sensors

$$\Delta\zeta_i = -\frac{r_i}{c}\sin(\phi_i)\tan(\phi_i - \phi_r - \phi_0)\Delta c \equiv a_i \Delta c. \tag{14}$$

The installation angle $\phi_0$ is zero for the EM 3000 on HUGIN 1000-MR. Finally we compute the covariance matrix, using $a_i$ defined in (14)

$$\boldsymbol{C}_c = E[\boldsymbol{w}_c \boldsymbol{w}_c^T] = \left\{a_i a_j \sigma_c^2\right\}_{i,j=1}^{m} \tag{15}$$

This shows the nature of the sound speed errors. It results in strongly correlated errors between beams with similar absolute beam angles, such as between the beams from starboard and port sides of HISAS 1030, but also between EM 3000 beams and HISAS 1030 beams in and near the overlap region. Since the HUGIN 1000-MR carries a CTD, and usually operates at low altitudes, this error is not dominant in our particular case. The error due to SSP errors are also considered to be small for the EM 3000 [20], as long as the error of the SSP has zero mean through the water column. The reason is that the errors caused by the SSP are canceled out when propagating the acoustic signal through the solution process of the ray equations. For the grazing angles of the HISAS 1030, the situation is different. The acoustic signal may propagate within the same SSP layer from transducer to the sea floor, and this may cause a bias in the measurements. The bias is again correlated between beams with similar absolute beam angles.

The error caused by not knowing the true terrain $h(x, y)$ but rather an estimate given by a DTM $\hat{h}(x, y)$ is also complicated. The error has both a stochastic component from errors in the estimates of the nodes forming the grid of the DTM, and a deterministic component from choice of interpolation for off-the-grid depths. A complete model of this error, requires knowledge of the correlation between all the node errors [23], although a parametric model using a variogram has been suggested in [24]. A simplified subset of the model for covariance caused by interpolation is described here. Consider a grid with regular north and east resolution $(\Delta x, \Delta y)$, and with nodes given by $\{(x_{i,j}, y_{i,j}, \hat{h}_{i,j})\}$, where $\hat{h}_{i,j}$ are all independent, and with errors zero-mean and Gaussian distributed with variance $\sigma_{\hat{h}}^2$. If we use bilinear interpolation for calculating two depths $\hat{h}_k$ at $(x_k, y_k)$, and $\hat{h}_l$ at $(x_l, y_l)$, both inside the the same grid cell $(i, j)$, we get [23]

$$\begin{aligned} E[\hat{h}_k \hat{h}_l] = \sigma_{\hat{h}}^2 ((1-\alpha_k)(1-\alpha_l)(1-\beta_k)(1-\beta_l) \\ + \alpha_k \alpha_l (1-\beta_k)(1-\beta_l) + (1-\alpha_k)(1-\alpha_l)\beta_k \beta_l \\ + \alpha_k \alpha_l \beta_k \beta_l), \end{aligned} \tag{16}$$

where $\alpha_k = (x_k - x_i)/\Delta x$ and $\beta_k = (y_k - y_i)/\Delta y$. Similar derivations can be made for the covariance between depth estimates in neighboring grid cells. For a complete model, (16) must be calculated for each grid point, along with the inverse of the complete covariance matrix, $\boldsymbol{C}^{-1}$. To reduce computation time, different parametric approximations to (16) are currently being tested. Using these approximations, $\boldsymbol{C}^{-1}$ only needs to be calculated once for each measurement update.

## IV. Experimental results

Terrain navigation based on (8) has been tested in post-processing on co-registered data from EM 3000 and HISAS 1030 collected by the HUGIN 1000-MR of the Royal Norwegian Navy in May 2010. The HUGIN 1000-MR was in this mission operated from HU Sverdrup II, FFI's own research vessel, and followed a route of variable terrain in the Oslo fjord, see Fig. 3. The operational altitude in this mission was set to 20 m, see Fig. 4.

The navigation data have been post-processed with NavLab

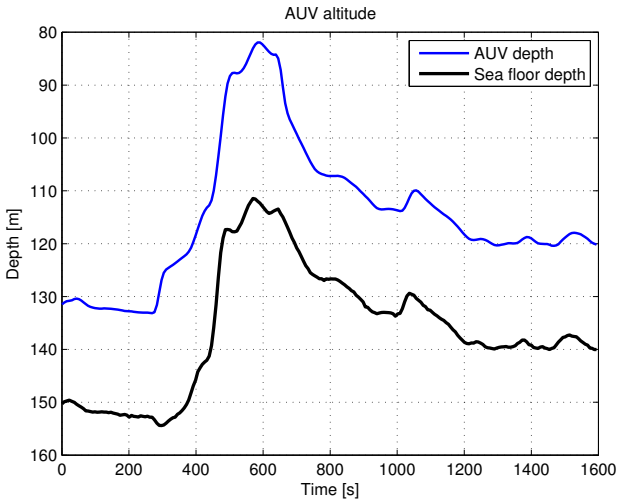


Fig. 4. The depth of HUGIN 1000-MR and sea floor depth, combined with the center beam of the EM 3000

[25] aided by acoustic position measurements from HiPAP on board the HU Sverdrup II. NavLab's navigation solution has a reported accuracy of about 1 m (1 $\sigma$ in both east and north) in this mission, and serves as a ground truth for the experiment. The reference DTM was based on EM 710 soundings collected by HU Sverdrup II, and processed by the automated grid generator of the HUGIN terrain navigation system [5]. A regular resolution of 10 m was chosen for this experiment. TerrLab [23] has been configured to run the PMF in the special mode described in Section III, and has been used to produce the results below. The grid of the PMF was set to 100 m x 100 m with a 1 m resolution. A batch of $K = 4$ measurements were used in the EM 3000 and the HISAS 1030 tests, while a batch of $K = 8$ was used in the test combining the two sensors. This approximately corresponds to a 1.1 s correlation period. Such a short period was chosen in this study to maintain the focus on the sensor measurements, rather than the algorithm's ability to improve accuracy by collecting a larger batch along the track. The results are therefore not representative for the expected accuracy when integrating this with the INS in the regular way, where $K$ would be of variable size depending on the amount of terrain information.

### A. Performance metrics

A set of metrics is calculated to quantify the performance of the PMF for the two sensors and their combination. The estimate of the AUV's position error is given by the minimum mean square error estimate (MMSE), i.e. by the first order moment of the filter PDF $p(\delta \boldsymbol{x}_K|Z_K)$, given by

$$\boldsymbol{\mu}_K = E[\delta \boldsymbol{x}_K] = \int_{G_K} \delta \boldsymbol{x}_K p(\delta \boldsymbol{x}_K|Z_K) d\delta \boldsymbol{x}_K. \quad (17)$$

TABLE I
SENSOR PERFORMANCE MEANS

| Sensors | $\bar{D}_{KL}$ | $\bar{D}_H$ | $\bar{\epsilon_e}$ | $\bar{\epsilon_n}$ | $\bar{\sigma}_{\epsilon,e}$ | $\bar{\sigma}_{\epsilon,n}$ |
|---|---|---|---|---|---|---|
| EM3000 | 2.07 | 0.25 | -1.10 | -0.10 | 8.14 | 7.12 |
| HISAS1030 | 4.38 | 0.16 | 0.18 | -1.59 | 5.39 | 2.87 |
| Both | 4.47 | 0.17 | 0.75 | -1.68 | 5.25 | 3.19 |

The covariance of this estimate is given by the second order moment $\boldsymbol{P}_K = E[(\delta \boldsymbol{x}_K - \boldsymbol{\mu}_K)(\delta \boldsymbol{x}_K - \boldsymbol{\mu}_K)^T]$, i.e.

$$\boldsymbol{P}_K = \int_{G_K} (\delta \boldsymbol{x}_K - \boldsymbol{\mu}_K)(\delta \boldsymbol{x}_K - \boldsymbol{\mu}_K)^T p(\delta \boldsymbol{x}_K|Z_K) d\delta \boldsymbol{x}_K. \quad (18)$$

The difference between the MMSE and the NavLab solution is denoted by $\epsilon_n$ for the northern direction, and $\epsilon_e$ for the eastern direction. The standard deviation of these differences are denoted respectively by $\sigma_{\epsilon,n}$ and $\sigma_{\epsilon,e}$.

To measure the amount of information gained from terrain navigation, the Kullback-Leibler divergence [26] from the initial PDF is introduced by

$$D_{KL} = \int_{G_K} p(\delta \boldsymbol{x}_K|Z_k) \log \frac{p(\delta \boldsymbol{x}_K|Z_K)}{p_0(\delta \boldsymbol{x}_K)} d\delta \boldsymbol{x}_K. \quad (19)$$

By inserting the assumption of a uniform initial PDF into (19), this leads to

$$D_{KL} = \log \frac{A_G}{\alpha} - \frac{1}{2} E[\boldsymbol{d}^T \boldsymbol{C}^{-1} \boldsymbol{d}]. \quad (20)$$

In this study we want to compare $D_{KL}$ for the different sensor configurations, and the higher the $D_{KL}$, the more information is gained from terrain navigation.

The last measure used, is the Hellinger distance [27] between the filter PDF and a Gaussian estimate of this PDF based on the first and second order moments. This approximation is denoted by

$$p_n(\delta \boldsymbol{x}_K) = N(\delta \boldsymbol{x}_K - \boldsymbol{\mu}_K, \boldsymbol{P}_K).$$

This is a measure of the similarity of the actual terrain navigation filter PDF and a corresponding Gaussian approximation that are proposed to be used by the Kalman filter of the INS. The square of the Hellinger distance is calculated by

$$D_H^2 = \frac{1}{2} \int_{G_K} \left( \sqrt{p(\delta \boldsymbol{x}_K|Z_k)} - \sqrt{p_n(\delta \boldsymbol{x}_K)} \right)^2 d\delta \boldsymbol{x}_K. \quad (21)$$

The Hellinger distance $D_H$ is a number between 0 and 1, where 0 means that the filter PDF is equal to a Gaussian PDF.

### B. Preliminary Results

The preliminary results are based on about 30 minutes of the data, where HUGIN 1000-MR traveled a track length of about 3 km. The mean results of the performance metrics are summarized in Table I. In this case, the inclusion of HISAS 1030 significantly increases the amount of information gained for terrain navigation. In addition the Gaussian approximation

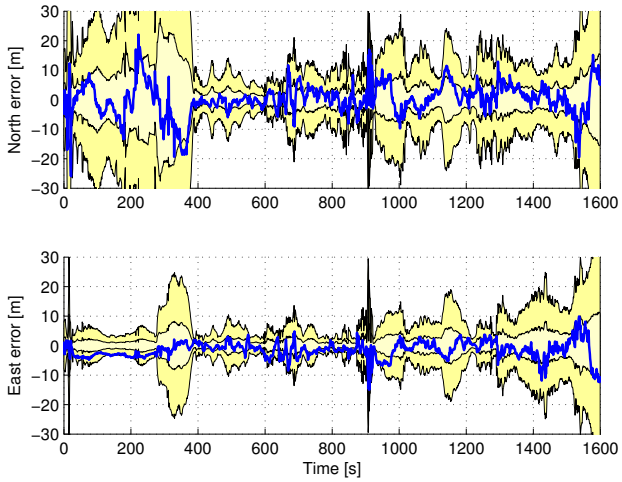


Fig. 5. Terrain navigation error (blue) using sidescan bathymetry from HISAS 1030, and the $\sigma$ (brighter yellow) and $3\sigma$ (darker yellow) confidence intervals of the Gaussian approximation $p_n(\delta \boldsymbol{x}_K)$.

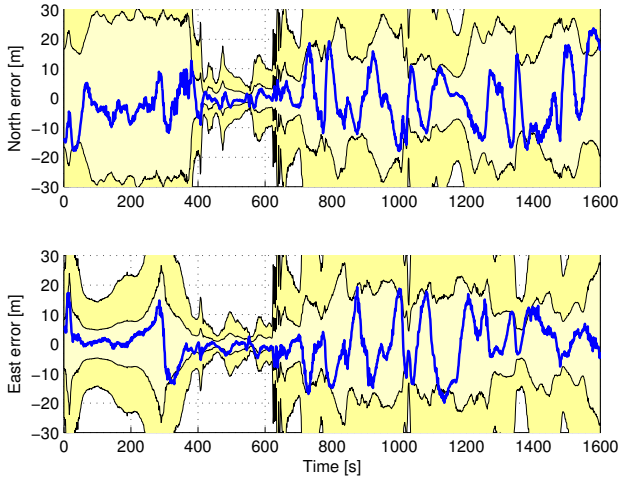


Fig. 6. Terrain navigation error (blue) using bathymetry from EM 3000, and the $\sigma$ (brighter yellow) and $3\sigma$ (darker yellow) confidence intervals of the Gaussian approximation $p_n(\delta \boldsymbol{x}_K)$.

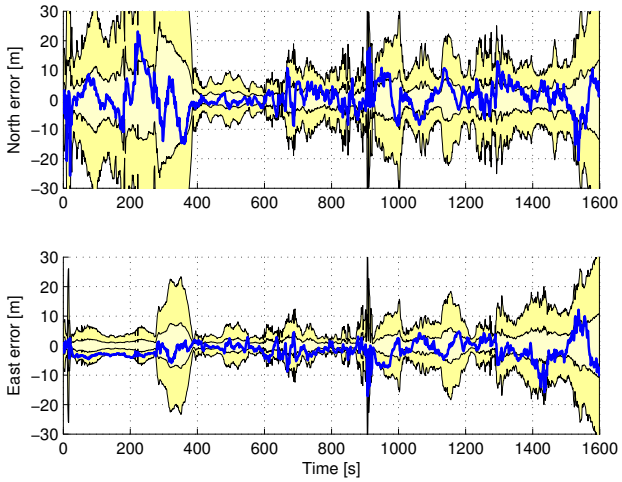


Fig. 7. Terrain navigation error (blue) using HISAS 1030 and EM 3000, and the $\sigma$ (brighter yellow) and $3\sigma$ (darker yellow) confidence intervals of the Gaussian approximation $p_n(\delta \boldsymbol{x}_K)$.

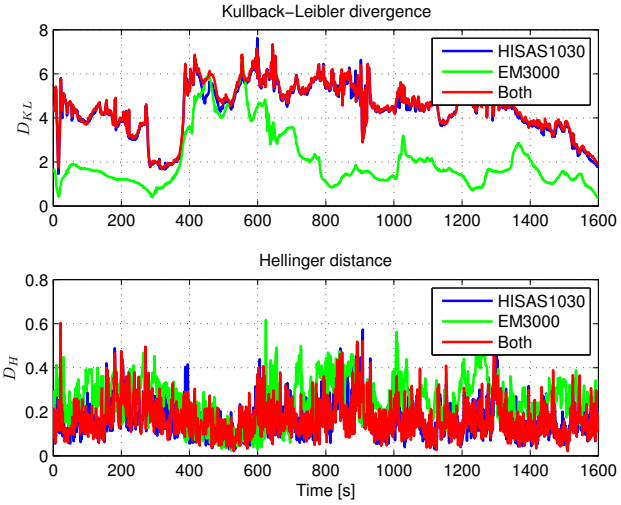


Fig. 8. Top: The Kullback-Leibler divergence of filter PDF $p(\delta \boldsymbol{x}_K|Z_k)$ from the uniform PDF $p_0(\delta \boldsymbol{x}_0)$. Bottom: The Hellinger distance between the filter PDF $p(\delta \boldsymbol{x}_K|Z_k)$ and the Gaussian approximation $p_n(\delta \boldsymbol{x}_K)$.

of the filter PDF seem to improve slightly. The mean bias of the terrain navigation error is low for all the three cases, but there is a moderate improvement of the variances for the cases including HISAS 1030. Surprisingly enough, there is no significant difference in performance for the combination of EM 3000 and HISAS 1030 versus using HISAS 1030 alone. This stems from the fact that there is very little terrain information for the EM 3000, see Fig. 8, except for a period between 400 s to 600 s, where a substantial improvement is also seen in the accuracy for the EM 3000 case in Fig. 6. By comparing the HISAS 1030 case in Fig. 5 and the fusion of the sensors in Fig. 7 in the same period, a slight improvement of the accuracy of combining the two sensors is also seen. In this period HUGIN 1000-MR encounters an underwater ledge along its path, and changes its altitude to about 30 m to go clear of the ledge, see Fig.4. The combination of increased terrain variation with increased altitude, gives a small period of very high accuracy for all the cases.

When comparing the estimated accuracy with the terrain navigation error for the EM 3000 in Fig. 6, the PMF seems in general to underestimate its own performance. On the other hand, the PMF seems in periods to slightly overestimate its performance when using HISAS 1030. There is also a small but consistent bias present in the terrain navigation error between 50 s to 300 s for the HISAS 1030 case in Fig. 5. This bias is not present in the EM 3000 case. The reason for the general over- and underestimation of the PMF, probably lies in the tuning of the error model, and with unmodeled effects. The bias may be caused by local problems with the DTM, the SSP or other parts of the processing that is not

completely common between the two sensors. These discrepancies are currently being investigated, and are important to solve if seeking optimal performance when combining two such accurate sensors for terrain navigation.

## V. Conclusion and future work

The challenges of terrain navigation in low altitude scenarios have been described, identifying the problem of too small ground-range coverage of the typical sensors used so far for terrain navigation. Operation at low altitudes are typical for the MCM-scenarios of the HUGIN 1000-MR AUVs. The inclusion of a side-looking interferometric sonar has been suggested to address the problem, such as the HISAS 1030, a sensor that is already part of the standard sensors carried by the HUGIN 1000-MR AUVs. A description of the sensor processing and parts of the error-modeling has been given. If optimal performance is to be maintained in the fusion of bathymetric measurements from high precision sensors such as the EM 3000 and HISAS 1030, knowledge of the covariance between the different error sources is essential. Some tests of terrain navigation have been presented on co-registered data from EM 3000 and HISAS 1030 at 20 m altitude. The preliminary results show an increase in performance using HISAS 1030 versus EM 3000, but little effect was seen in fusing the two sensors. The main reason for this was that the AUV traveled directly over the flatter parts of the terrain, leaving most of the variable topography outside the coverage of the EM 3000.

Future work will include improving the covariance model further, and identifying some terrain navigation error biases found in the tests with data from HISAS 1030. Further terrain navigation tests will also be performed on data collected during operations with an optical camera, typical at 5 m altitude. It is expected that the improvement by additionally using HISAS 1030 for terrain navigation, is substantial in those scenarios.

## Acknowledgment

The authors thank the crew onboard HU Sverdrup II, and the HUGIN operators at FFI for the collection of the data.

## References

[1] B. Jalving, K. Gade, O. Hagen, and K. Vestgård, "A toolbox of aiding techniques for the HUGIN AUV integrated inertial navigation system," in *Proceedings of the IEEE Oceans 2003*, San Diego, CA, 2003.

[2] P. Hagen, Ø. Hegrenæs, B. Jalving, Ø. Midtgaard, M. Wiig, and O. Hagen, *Underwater Vehicles*. Vienna, Austria: In-Tech Education and Publishing, 2009, ch. Making AUVs Truly Autonomous, pp. 129–152.

[3] J. Carlström, "Results from sea trials of the Swedish AUV62F's terrain navigation system," in *15th International International Symposium on Unmanned Untethered Submersible Technology (UUST'07)*, Durham, NH, USA, 2007.

[4] D. Meduna, S. Rock, and R. McEwen, "Low-cost terrain relative navigation for long-range AUVs." in *MTS/IEEE Oceans 2008 Conference*, Quebec City, QC, Canada, September 2008.

[5] O. Hagen, K. Ånonsen, and M. Mandt, "The HUGIN real-time terrain navigation system," in *Proceedings of the MTS/IEEE Oceans 2010 Conference*, Seattle, WA, USA, September 2010.

[6] K. Ånonsen and O. Hagen, "An analysis of real-time terrain aided navigation results from a HUGIN AUV." in *Proceedings of the IEEE/ION Oceans 2010 Conference*, Seattle, WA, September 2010.

[7] D. Meduna, S. Rock, and R. McEwen, "Closed-loop terrain relative navigation for AUVs with non-inertial grade navigation sensors," in *Autonomous Underwater Vehicles (AUV), 2010 IEEE/OES*, Monterey, CA , USA, 2010.

[8] K. Ånonsen and O. Hagen, "Recent developments in the HUGIN AUV terrain navigation system," in *Proceedings of the MTS/IEEE Oceans Conference 2011*, Kona, HI, USA, September 2011.

[9] T. Fossum, T. Sæbø, B. Langli, H. Callow, and R. Hansen, "HISAS 1030 - high resolution interferometric synthetic aperture sonar," in *Proceedings of the Canadian Hydrographic Conference and National Surveyors Conference*, Victoria, BC, Canada, May 2008.

[10] T. Sæbø and B. Langli, "Comparison of EM 3000 multibeam echo sounder and HISAS 1030 interferometric synthetic aperture sonar for seafloor mapping," in *ECUA*, 2010.

[11] T. O. Sæbø, "Seafloor depth estimation by means of interferometric synthetic aperture sonar," Ph.D. dissertation, University of Tromsø, September 2010.

[12] Ø. Hegrenæs, T. O. Sæbø, P. E. Hagen, and B. Jalving, "Horizontal mapping accuracy in hydrographic AUV surveys," in *Proceedings of the IEEE Autonomous Underwater Vehicles 2010*, Monterey, CA, USA, September 2010.

[13] K. Ånonsen and O. Hagen, "Terrain aided underwater navigation using pockmarks," in *Proceedings of the MTS/IEEE Oceans Conference*, Biloxi, MS, October 2009.

[14] R. Bucy, "Bayes theorem and digital realizations for non-linear filters," *The Journal of the Astronautical Sciences*, vol. XVII, no. 2, pp. 80–94, Sep.-Oct. 1969.

[15] R. Bucy and K. Senne, "Digital synthesis of non-linear filters," *Automatica*, vol. 7, no. 3, pp. 315–322, May 1971.

[16] N. Bergman, L. Ljung, and F. Gustafsson, "Terrain navigation using Bayesian statistics," *IEEE Control Systems Magazine*, vol. 19, no. 3, pp. 33–40, Jun. 1999.

[17] K. Ånonsen, "Advances in terrain aided navigation for underwater vehicles," Ph.D. dissertation, Norwegian University of Science and Technology, 2010.

[18] W. Baker and R. Clem, "Terrain contour matching (TERCOM) primer," Wright Patterson Air Force Base Aeronautical Systems Division (1977), OH, USA, Tech. Rep., 1977.

[19] I. Nygren and M. Jansson, "Terrain navigation for underwater vehicles using the correlator method," *Oceanic Engineering, IEEE Journal of*, vol. 29, no. 3, pp. 906 – 915, july 2004.

[20] E. Hammerstad, "Multibeam echo sounder accuracy," Kongsberg Maritime, Horten, Norway, EM Technical Note, February 1998.

[21] R. Hare, "Depth and position error budgets for multibeam echosounding," *International Hydrographic Review*, vol. 72, no. 2, September 1995.

[22] O. Hagen and B. Jalving, "Vertical position estimation for underwater vehicles," *Sea Technology*, no. 12, pp. 51–54, Dec. 2008.

[23] O. Hagen, "TerrLab - a generic post-processing tool for terrain referenced navigation," in *MTS/IEEE Oceans Conference 2006*, Boston, MA, USA, September 2006.

[24] D. Meduna, S. Rock, and R. McEwen, "AUV terrain relative navigation using coarse maps," in *Proc. 16th International Symposium UUST09*, Durham, New Hampshire, USA, 2009.

[25] K. Gade, "NavLab, a generic simulation and post-processing tool for navigation," *European Journal of Navigation*, vol. 2, no. 4, pp. 51–59, November 2004. [Online]. Available: www.navlab.net

[26] S. Kullback and R. Leibler, "On information and sufficiency," *Annalls of Mathematical Statistics*, vol. 22, pp. 79–86, 1951.

[27] R. Beran, "Minimum hellinger distance estimates for parametric models," *The Annals of Statistics*, vol. 5, pp. 445–463, 1977.